Applied Surface Science 493 (2019) 423–430

Contents lists available at ScienceDirect

Applied Surface Science

journal homepage: www.elsevier.com/locate/apsusc

Full length article

Switching off the SERS signal for highly sensitive and homogeneous detection of glucose by attenuating the electric field of the tips

Li Zhang[a], Xiaodan Li[a], Yunyu Jin[a], Youlin Zhang[b], Xiaomin Liu[b,d], Yulei Chang[b], Lijun Xu[a,*], Huiying Zhao[a,*], Langping Tu[b], Dan Wang[c], Xianggui Kong[b], Bin Xue[b,c,**]

[a] The First Hospital, Jilin University, Changchun 130021, PR China
[b] State Key Laboratory of Luminescence and Applications, Changchun Institute of Optics, Fine Mechanics and Physics, Chinese Academy of Sciences, Changchun 130033, PR China
[c] Key Laboratory of Optoelectronic Devices and Systems of Ministry of Education and Guangdong Province, College of Physics and Optoelectronic Engineering, Shenzhen University, Shenzhen 518060, PR China
[d] State Key Laboratory on Integrated Optoelectronics, College of Electronic Science and Engineering, Jilin University, Changchun 130012, PR China

ARTICLE INFO

Keywords:
SERS
Glucose sensing
Homogeneous phase
Silver nanotriangle

ABSTRACT

The advances in surface-enhanced Raman scattering (SERS) have resulted in significant improvements for sensing glucose, achieving a highly detecting sensitivity of the order of μM. Highly sensitive glucose detection, however, is still a challenge due to extremely small Raman scattering cross section of glucose molecules and weak interaction between the molecules and the metal nanoparticles. Here, we designed a novel homogeneous SERS-based nanoplatform composing of the SERS tags and glucose oxidase in aqueous solution for a highly sensitive glucose detection. Adding glucose caused enzymatic oxidation reaction to etch the tip electric field (E) of silver nanotriangle. Thus, the decreased intensity of E was greatly amplified by the change of SERS signal (E^4 dependent), which resulted in an excellent glucose detection limit of 0.4 nM was firstly achieved. Furthermore, the nonlinear relationship between the decreased SERS intensity and the glucose concentrations was reasonably revealed based on theoretical calculations and deeply understanding of the enhancement mechanism, which is very useful in improving the sensitivity and accuracy of trace glucose detection. The as-prepared nanoplatform showed good sensitivity and high selectivity only through observing the SERS intensity change, which is potential for highly sensitive and practical glucose detection for clinical trace analyses.

1. Introduction

Glucose is one of the important metabolites which serve as a vital role in life processes and disease diagnosis [1]. The deficiency or excess of the glucose is directly related to the incidence and evolution of diabetes mellitus which is a serious threat to human health, including higher risks of heart disease, kidney failure, impairment of lung functions, or blindness [2]. Therefore, developing sensitive detection method for glucose is of great importance for early diagnosis and control of diabetes mellitus. Accordingly, various optical approaches for detecting glucose have been developed [3,4]. Among them, surface enhanced Raman scattering (SERS), an enhanced effect of the localized surface plasmon resonances (LSPR) on a roughened noble mental particle surface on Raman scattering of molecules, is the most promising in the detection of trace biomolecules due to its high specificity and sensitivity for the recognition and detection of molecules [5–10], pathogens [11–13], cells [14]. Particularly, most Raman scattering peaks possess a very narrow full width at half maximum (FWHM), which is suitable for multicomponent analysis and imaging [15,16]. Recent advances in the research of noble metal SERS substrates [17–19], have also led to significant improvements in glucose detection [5,20]. However, highly sensitive SERS detection for glucose in aqueous solutions remains a challenging due to extremely small Raman scattering cross section (10^{-30} cm^2/sr) of glucose and extremely weak binding affinity between the molecules and the metal nanoparticles [4]. Although there have been many reports on excellent label-free SERS detection of glucose, the sensitivity of the reported glucose detection was almost at the level from μM to mM [5,20,21], the process of analyzing

* Corresponding authors.
** Correspondence to: B. Xue, State Key Laboratory of Luminescence and Applications, Changchun Institute of Optics, Fine Mechanics and Physics, Chinese Academy of Sciences, Changchun 130033, PR China.
E-mail addresses: ljxu@jlu.edu.cn (L. Xu), hui_ying@jlu.edu.cn (H. Zhao), xuebin2021@szu.edu.cn (B. Xue).

https://doi.org/10.1016/j.apsusc.2019.07.053
Received 3 June 2019; Received in revised form 22 June 2019; Accepted 7 July 2019
Available online 08 July 2019
0169-4332/

meaningful data from the rich information acquired in the SERS spectra of biomolecules is too complicated to be analyzed availably. Recently, to overcome the weak binding affinity of glucose, bisboronic acids as receptors were used to capture glucose for SERS substrates [22,23]. Very recently, SERS tags containing boronic acid group to capture glucose were further developed for highly sensitive sensing of glucose [24]. Moreover, mercaptophenylboronic acid and albumin were used to capture glucose on the SERS substrates, respectively [25,26]. Therefore, due to the anomeric effect of glucose, it is still difficult to develop highly sensitive SERS-based glucose sensor.

Although various SERS substrates have been used for detecting glucose, the repeatability of constructing SERS substrates is still one of the most difficult problems to be solved in developing SERS methods [5]. As an alternative solution, the homogeneous detection is a "mix and measure" method that depends on the generating optical sensing signal in the whole volume of the homogeneous analyte solution [27], without the need of a highly repeatable construction of SERS substrates, in which the sensing signal probes are homogeneously blended with the analyte solution. Such simple method of the homogeneous detection offers many advantages for point-of-care detecting applications owing to effectively reducing requirements for the repeatability of the surface structure of the substrate and/or sample preparation. In addition, planar plasmonic substrates often occupy a large proportion of the plasmonic near-field [28], resulting in a reduced sensitivity. While plasmonic nanoparticles in homogeneous solution will have three-dimensional plasmonic electric field for highly sensitive SERS sensing. Moreover, compared with the SERS detection widely based on substrates, The analyte molecules diffuse with a three-dimensional in a homogenueous solution and are captured by the signal sensing probes for the homogeneous SERS methods, instead of the two-dimensional diffusion in the SERS substrate, which is very useful for the capture of the molecules by sensing elements [29]. Numerous homogeneous biodetection methods that employ particles, such as Au or Ag, magnetic beads, and fluorescence particle labels, etc., have been developed based on different optical principles, for example, fluorescence polarization [30], fluorescence correlation spectroscopy [31], and Förster resonance energy transfer [32,33]. Moreover, a few of articles on homogeneous SERS detection were reported for biomolecules, e.g. antibody-fragments-decorated Au nanoparticles, achieving a detection limit of 0.5 pM for cytokine [34]. However, so far, there have been few reports on SERS methods for detecting glucose in a homogenously mixed aqueous solution.

Here, a novel homogenous silver nanotriangle-based SERS nanoplatform (HSTSN) consisting of glucose oxidase (GOx) and SERS tags of silver nanotriangles (SNTs) coordinated with the thiol of *p*-aminothiophene (*p*-ATP) in aqueous solution was proposed and constructed for detecting glucose. Unlike most label-free SERS to sense the glucose with the weak signal and weak binding affinity, we utilized the drastic change in the intensity of the highly strong local electric field (*E*) at the tips of SNTs leads to sharply decay the SERS signal to highly sensitive detection of glucose, which reached by etching of H_2O_2 generated by enzymatic oxidation reaction GOx to capture glucose, rather than the one on the round after etching the SNTs which is currently reported. The highly sensitive sensing of glucose was fulfilled due to combining the advantages of the highly strong local electric field (*E*) at the tips of the SNT_S, the high Raman activity of the *p*-ATP, the high sensitivity of the etching of H_2O_2 generated from glucose to the tips of the SNTs and the three-dimensional diffusion of H_2O_2 in aqueous solution. In addition, it is well noted that SERS enhancement are fourth power dependent of the local electric field [7], showing the relationship between the SERS intensity and the concentration of analyte molecules should be nonlinear in theory. Although the nonlinear relationship between SERS intensity and concentration of detecting molecules in a few of reports was observed, how to use the nonlinear relationship has not been discussed at all [22,26]. Therefore, it remains a new challenge how to apply the relationship between the intensity of SERS and the concentration of the detection molecules, which is influenced by the nonlinear relationship between SERS and the tip electric field. Here, the nonlinear relationship between the SERS intensity and the low concentration of glucose was revealed and employed, which was fully supported by the theoretical calculations. Thus, for the first time to the best of our knowledge, the HSTSN was able to detect glucose as low as 0.4 nM. Our findings show great potential for the development of highly sensitive SERS methods for detecting glucose in homogeneously aqueous solution, without SERS substrates.

2. Experimental section

2.1. Chemicals and materials

Silver nitrate ($AgNO_3$, ≥99.8%), trisodium citrate (≥99%), poly (vinylpyrrolidone) (PVP, $M_w \approx 30,000$ g/mol) were obtained from Beijing Chemical Works, sodium borohydride ($NaBH_4$, ≥98%), *p*-aminothiophenol (*p*-ATP, ≥90%), glucose oxidase (GOx) were purchased from Sigma-Aldrich. Glucose, fructose, maltose, sucrose, and starch were purchased form Aladdin. Water was distilled and deionized using a Millipore Milli-Q Purification System, which has a resistivity of not less than18.2 MΩ. All chemicals were obtained from commercial sources and used without further purification.

2.2. Synthesis of SNTs

SNTs were synthesized similar to the method reported by Yin et al [35]. 93 ml deionized water, $AgNO_3$ (10 mM, 1 mL), and trisodium citrate (15 mM, 1 mL), PVP (1.75 mM, 4 mL), H_2O_2 (30 wt%, 240 μL) were mixed under vigorously stirring at room temperature. 1 mL $NaBH_4$ (100 mM) was quickly added into this mixture. About 30 min later, the solution turned gradually from achromatism to yellow, and blue, showing the formation of SNTs. The as-prepared SNTs were ~70 nm in length of the sides.

2.3. Fabrication of SERS tags

p-ATP molecules are usually used for SERS, owning to their strong coordination ability with noble metal nanoparticles and large Raman scattering cross section [36]. Here, *p*-ATP was used to fabricate SNTs-based SERS tags. The as-prepared SNTs were firstly centrifugated (10,000 rpm, 15 min) from solution and washed for three times to exclude the unreacted agents and the PVP ligands from the surface of the SNTs as much as possible, then dispersed again into 1.8 mL deionized water. Next, the 1.8 mL of the purified SNTs solution (0.16 nM) were mixed with the 200 μL *p*-ATP (100 μM) ethanol solution for 12 h to coordinate thiol of *p*-ATP to Ag of the SNTs surface for obtaining SERS tags. Finally, the SNTs/*p*-ATP were further washed with water and ethanol, and re-dispersed into 10 mL aqueous solution for obtaining SERS tags.

2.4. SERS detection for glucose

For the homogeneous SERS detection of glucose, the HSTSN was firstly prepared by mixing SERS tags of 180 μL SNTs/*p*-ATP with 20 μL GOx (0.5 mg/mL) with 2 mL deionized water, to obtain the HSTSN (SNTs/*p*-ATP-GOx) for detecting glucose. The SERS of the HSTSN (SNTs concentration ~0.028 nM) incubated with 100 μM glucose for different time were measured, respectively, within the incubation time range of 0–80 min, to determine the end time of the complete oxidation of 100 μM glucose. The different concentration (10–100 μM) of glucose was added in the same HSTSN condition to detection, respectively. For highly sensitive glucose sensing, HSTSN (SNTs concentration ~0.014 pM) incubated with different concentration (0–100 nM) of glucose for 60 min, and then the SERS spectra were record for sensing analysis. In the control experiments, 500 μM of fructose, lactose and maltose were

added into the HSTSN, respectively, under the same conditions mentioned above to estimate the specificity for detecting glucose.

2.5. Finite-difference time-domain (FDTD) simulations

The FDTD simulations were performed by utilizing a commercial software (FDTD solutions, Lumerical Solutions) to understand the *E* distributions of SNTs. The structures were excited with polarized plane-wave light (Fig. S1). A mesh size of 1 nm in the nanoparticle region was performed. The sizes of SNTs and other shape of nanoparticles were set in Fig. S1. The dielectric function of SNTs was taken from Ag-CRC in the material library of the software. The refractive index of the medium was set at 1.333 to mimic water. Perfectly matched layer (PML) was used as the boundary conditions in FDTD simulations.

2.6. Instrument and characterizations

Ultraviolet-visible (UV–VIS) absorption spectra were acquired by using a UV-3101PC scanning spectrophotometer (Shimadzu). Scanning electron microscope (SEM) analysis of SNTs samples was performed on a field emission scanning electron microscopy (FESEM, Hitachi, S-4800). For SERS measurement, a 785 nm fiber-coupled laser diode (InPhotonics, 100 mW) was used for excitation, and a spectrometer (QE 65 pro) with thermoelectric cooled CCD was used to collect Raman signal. Raman spectra were obtained through combining a 105 μm excitation fiber and a 200 μm collection fiber.

3. Results and discussion

3.1. Principle of SERS assay based on HSTSN

To achieve high sensitivity of a homogeneous detection of glucose, a novel HSTSN consisting of GOx and SERS tags in aqueous solution was constructed by combining these advantages of the sensitive etching of H_2O_2 to the tips of SNT_S, highly strong *E* at the tips of the SNT_S and three-dimensional diffusion interaction between H_2O_2 and SNT_S in aqueous solution. The principle schematic of the HSTSN to detect glucose was shown in Scheme 1. The SERS tags composing of SNTs coordinated with *p*-ATP, and the GOx are homogeneously dispersed in aqueous solution, which constitutes a novel HSTSN. When glucose is added into the HSTSN, the specially catalytic reaction between GOx and glucose will produce H_2O_2 which sensitively etches the tips of the SNTs, leading to the shape of SNTs from the triangle to the round, resulting in the drastic decrease of the *E* intensity at the tips, and causing a sharp decline in the intensity of the SERS due to the dependent relationship between $|E|^4$ and SERS intensity, as shown in the Scheme 1. Therefore, the high sensitivity of glucose detection will be reached.

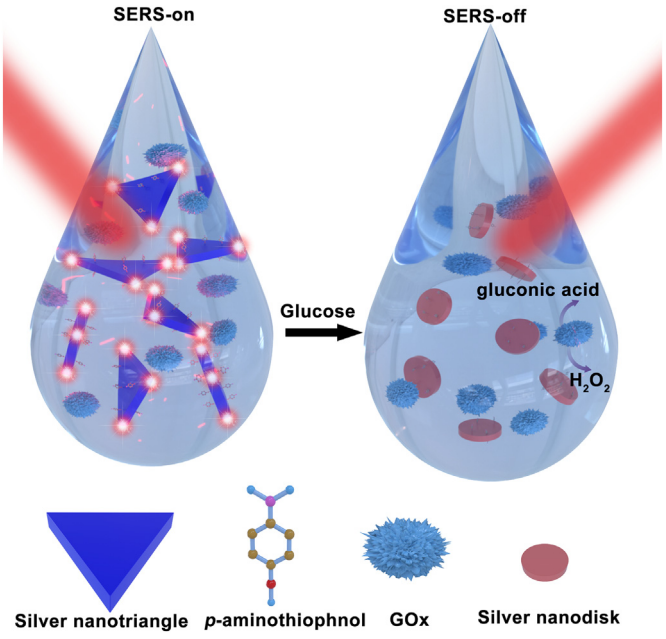

Scheme 1. Schematic illustration of the SNTs-based HSTSN for detecting glucose.

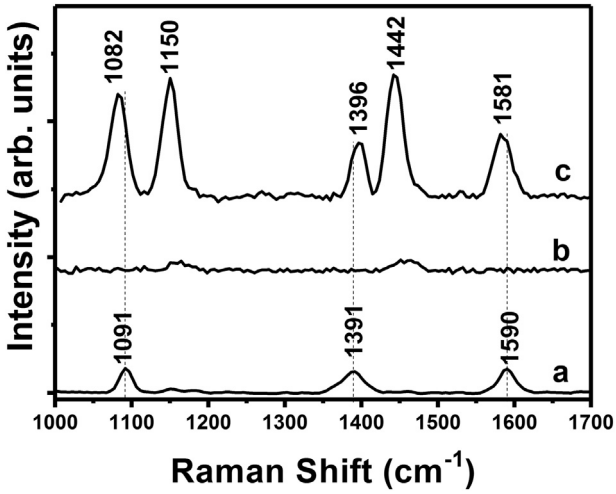

Fig. 1. Raman spectra of *p*-ATP (50 mM) in aqueous solution with 50 mM NaOH (a), and SERS of *p*-ATP recorded in the HSTSN (SNTs/*p*-ATP-GOx) incubated for 60 min with (b) and without 100 μM glucose (c), respectively. The accumulation time of QE 65 Pro spectrometer was set to100 ms for acquiring SERS spectra.

For investigation of the SERS sensing of the HSTSN to glucose, Raman spectra of *p*-ATP in aqueous solution (a), SERS of the HSTSN containing glucose (b) and not containing glucose (c) were detected and analyzed in the wavenumber range of 1000–1700 cm^{-1}, respectively, as shown in Fig. 1. The five strong SERS bands at 1082, 1150, 1396, 1442 and 1581 cm^{-1} were observed under the excitation of 785 nm laser. Besides the SERS band at 1082 cm^{-1} (a_1 vibration modes), the other four bands were identified as the vibration of b_2 modes [36]. By comparing the SERS of the SNTs/*p*-ATP-GOx (c) with Raman spectra of *p*-ATP (a) in Fig. 1, it can be clearly found that the SERS peak at 1396 cm^{-1} showed a blue-shift relative to the one at 1391 cm^{-1} (a), the peak at 1581 cm^{-1} exhibited a red shift relative to that one at 1590 cm^{-1}(a), and the intensity of the SERS bands was obviously enhanced relative to the Raman spectra (a), which resulted mainly from the strong interactions between the assembled *p*-ATP and SNTs and the according SERS effect. The vibration peaks (1150 and 1442 cm^{-1}) may come from the chemical coupling transformation of *p*-ATP [36], or charge-transfer mechanism [37]. Compared with the SERS intensity (c) of the HSTSN without glucose, the intensity of the SERS (b) was much weaker than the one of the SERS (c) after the HSTSN incubated with 100 μM glucose for 60 min, suggesting that the HSTSN was highly effective in sensing glucose. Moreover, due to the SERS tags were uniformly mixed and dispersed in the homogeneous solution, the small test deviation was achieved (1.39%) from different measurements at different positions of the solution (Fig. S2), which indicated the good repeatability of the nanoplatform.

3.2. Mechanistic investigation

To understand the mechanism of HSTSN sensing to glucose, we firstly monitored the absorption spectra changes of the samples. As shown in Fig. 2a in which the absorption peaks, at ca. 753 nm and 325 nm, and one shoulder at 502 nm, respectively, were assigned to the in-plane dipole, the out-of-plane quadrupole plasmon resonance, and

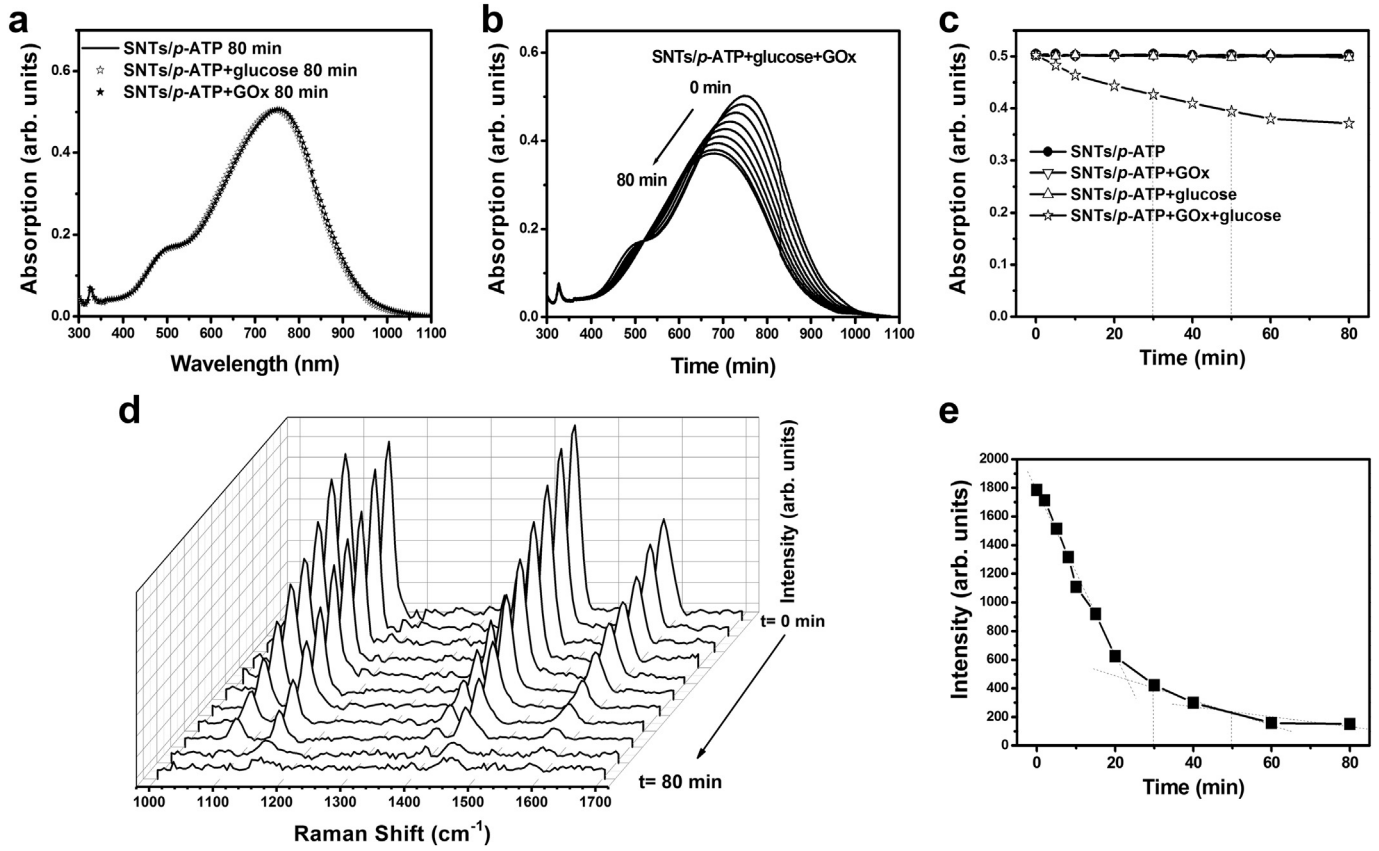

Fig. 2. (a) UV–Vis absorption spectra of the three samples (SNTs/p-ATP, SNTs/*p*-ATP-GOx, and SNTs/*p*-ATP-glucose) with 0.028 nM of concentration of SNTs after incubation for 80 min. (b) Time-dependent UV–Vis absorption spectra of the SNTs/*p*-ATP-GOx-glucose (100 μM) nanoplatform at different incubation time in the range of 0–80 min. (c) The intensity of the absorption peak of the four samples (i.e. SNTs/*p*-ATP, SNTs/*p*-ATP-GOx, SNTs/*p*-ATP-glucose, and SNTs/*p*-ATP- GOx-glucose) vs incubation time. (d) SERS spectra of the HSTSN (SNTs (0.028 nM)/*p*-ATP-GOx) incubated with 100 μM glucose at different incubation time (from 0 to 80 min), the accumulation time of the spectra was 100 ms. (e) Plots of the intensity of the SERS peak at 1442 $cm^{-1}$of the HSTSN vs the incubation time.

the in-plane quadrupole resonance of SNTs, respectively [38,39]. After incubation for 80 min, comparing the absorption spectra of SNTs/*p*-ATP with the ones of the SNTs/*p*-ATP-GOx and SNTs/*p*-ATP-glucose (Fig. 2a and c), it can be seen that there was little change in the absorption spectra among three samples, indicating that neither GOx nor glucose could react with the SNTs/*p*-ATP alone. To examine the sensing characteristics of the SNTs/*p*-ATP-GOx to glucose, we monitored the changes of the time-dependent absorption spectra of the SNTs/*p*-ATP-GOx-glucose in the range from 0 to 80 min (Fig. 2b and c). The blue-shift of absorption peak from ca.753 to 670 nm and the decrease in intensity of the LSPR absorption band were observed as the evolution of the time, which originated from the continuously etching effect of H_2O_2, generated by the enzymatic oxidation of glucose by GOx, on SNTs. The reactions between glucose and GOx can be explained as follows by Eqs. (1) and (2) [40,41]:

$$\text{glucose} + O_2 + H_2O \xrightarrow{GOx} \text{gluconic acid} + H_2O_2 \quad (1)$$

$$2Ag + H_2O_2 \rightarrow 2Ag^+ + 2OH^- \quad (2)$$

The etching of the SNTs will intensively decrease the sharpness of their tips and anisotropic ratio, which leads to the blue-shift of the peak position and the decrease in the intensity of the in-plane dipole plasmon resonance absorption band. Besides the results in Fig. 2, the etching effect of H_2O_2 on the SNTs was confirmed by SEM images, in which the shape of SNTs observably changed from larger triangle to smaller round plates after adding glucose (Fig. 3). It is well known that there was a stronger *E* at the tips of the SNTs than on the surface of round Ag nanoparticles, which could nonlinearly amplify SERS signal (Fig. 1c) because the enhancement of the SERS is proportional to the fourth power of local electric field. It is obvious that as long as H_2O_2 has an extremely slight etching to the tips of the SNT_S, which not only results in a change in the LSPR absorption intensity of the SNTs, but also leads to a blue-shift of the absorption band. Importantly, the large blue-shift will lead to a large deviation of LSPR absorption band from the resonant excitation wavelength, which will sharply lower the SERS intensity. Therefore, the SERS sensing based on the HSTSN are very sensitive to glucose.

The time-dependent SERS of the HSTSN incubated with glucose in the range of 0–80 min was also investigated. Fig. 2d and e showed that the intensity of SERS of the HSTSN decreased as the increase in incubation time, which reached a stable minimum at ca. 60 min, and no longer decreased as the increase of incubation time in the range of 60 to 80 min, indicating that the reaction time should be set about 60 min. Interestingly, it can be found that the changes of SERS intensity (Fig. 2e) dropped faster than the changes of absorption intensity (Fig. 2c), which can be explained below.

To better understand the enhanced mechanism of the SERS which based on the amplified *E* of the SNTs, FDTD simulations were used to evaluate the distributions of the *E* on the SNTs. Fig. 4 clearly shows that the strongest *E* is localized at the tips of SNTs. When the shape of SNTs gradually changes from triangle to round due to the continuously etching effect of H_2O_2, for example, the intensity of *E* significantly decreases at the tips (Fig. 4), leading to the decline of SERS intensity, which agrees well with experimental observations as shown in Fig. 1. Simulated results of Fig. S3 show the blue-shift of the absorption spectra as the tips of the SNTs are truncated, which also agrees well with experimental observations (Fig. 2b). Due to SERS is $|E|^4$ enhancement dependent [7], we also simulated the distributions of the

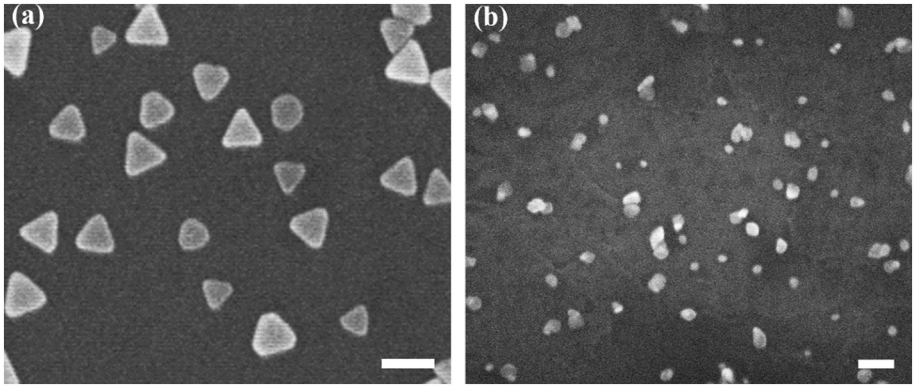

Fig. 3. SEM images of SNTs in the HSTSN before (a) and after (b) incubation with glucose (100 μM). All scale bars are 100 nm.

$|E|^4$ of SNTs with varying degrees of truncation tips (Fig. 4b). The results are obtained that the value of $|E|^4$ (Fig. 4b) diminishes faster than that of $|E|^2$ (Fig. 4a). Due to the plasmonic absorption is $|E|^2$ dependent and SERS is $|E|^4$ dependent, therefore, the SERS intensity will diminish faster than the absorption intensity, which agrees well with experimental results (Fig. 2c and e). Apparently, when the value of E is falling off a little, the SERS intensity will evidently lower. Therefore, the SERS intensity will be highly sensitive to the minor change of the E intensity at the tips of the SNTs, which is beneficial to highly sensitive sensing.

3.3. Sensing analysis based on the HSTSN

We further studied the sensitivity of the as-prepared HSTSN for glucose detection. Fig. 5A shows the absorption spectra of the three HSTSN with SNTs concentration of 0.14 nM (a), 0.028 nM (b), and 0.14 pM (c), respectively. When the SNTs concentration diluted 5 times from original 0.14 nM to 0.028 nM, the absorption of SNTs was visible. At this condition, colorimetric sensing to glucose (similar to the data shown in Fig. 2b) and SERS sensing to glucose (Fig. S4) could be simultaneously fulfilled. But when the concentration of SNTs diluted 1000 times from original 0.14 nM to 0.14 pM, the absorption (c) of the

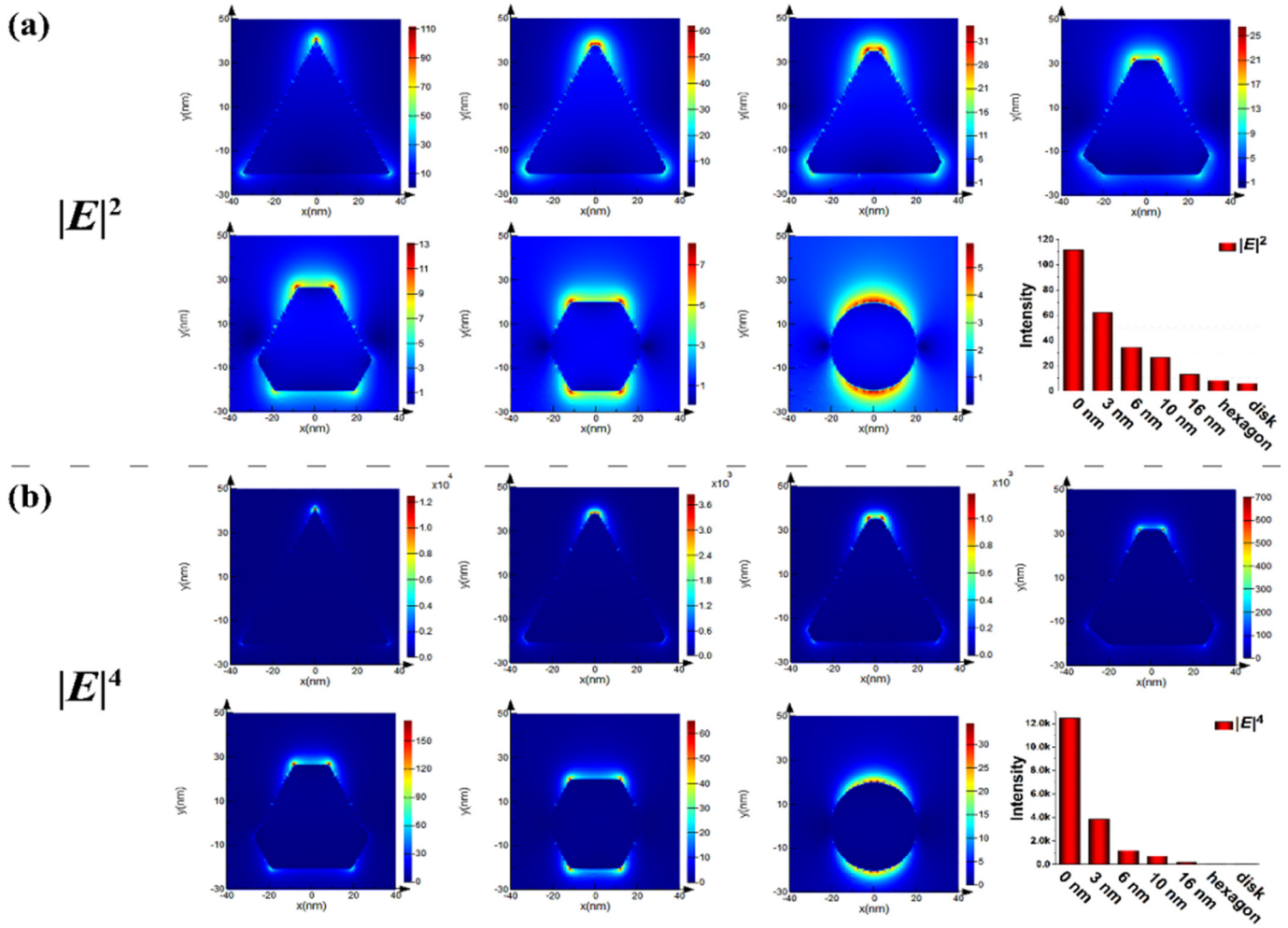

Fig. 4. Distributions of the $|E|^2$ (a) and the $|E|^4$ of on SNTs with varying degrees of truncation tips, achieved by using FDTD simulation.

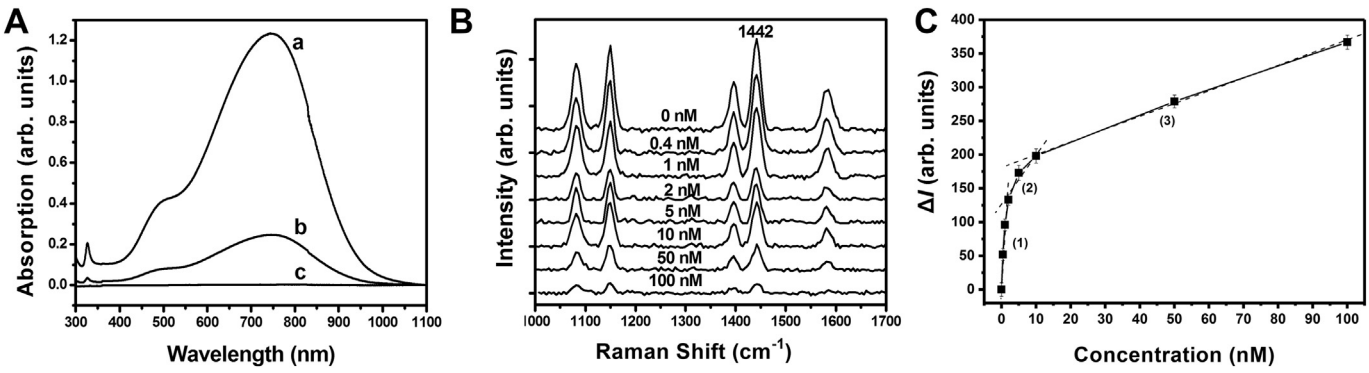

Fig. 5. (A) absorption spectra of the HSTSN with 0.14 nM (a), 0.028 nM (b), 0.14 pM (c) of the SNTs, respectively. (B) SERS spectra of the HSTSN incubated with different concentration (0–100 nM) of glucose, accumulation time was 1 s. (C) plots of intensity change ($\Delta I = I_0 - I$) of the SERS peak at 1442 cm^{-1} vs concentration, $\Delta I = I_0 - I$, I_0 and I represented the SERS intensity before and after incubation with different concentration of glucose. The error bars were from the three measurements. The linear coefficients of correlation were 0.981, 0.962, 0.998 for region (1), (2), (3), respectively.

Table 1
Comparison of recently reported SERS methods for sensing glucose.

Method	Sensing system	Measured signal	LOD	Reference
Label-free SERS	Ag NPs-Si substrate	Intensity increase	0.28 mM	21
Label-free SERS	Ag NPs/PDDA/GOx substrate	Intensity decrease	1 μM	42
Label-free SERS	Plasmonic cavity/PDMS	Intensity increase	1 mM	43
Label-free SERS	Albumin coated Au nanostar substrate	Intensity increase	1 nM	26
Labelled SERS	MPBA tagged Au/Ag coated polystyrene substrate	Intensity increase	100 μM	22
Labelled SERS	CPBA tagged Au@Ag nanorod substrate	Intensity increase	10 nM	24
Labelled SERS	*p*-ATP tagged SNTs/GOx	Intensity decrease	0.4 nM	This work

APBA, 3-aminophenyl boronic acid; *PDDA*, poly(dimethyldiallyl ammonium chloride); *PDMS*, poly(dimethylsiloxane); *MPBA*, 4-mercaptophenylboronic acid; *CPBA*, 4-cyanophenylboronic.

SNTs could not be observed (Fig. 5A). While at the same condition, the strong SERS spectra of the HSTSN could still be easily detected for sensing glucose (Fig. 5B), which demonstrated that the SERS sensing strategy was more sensitive than colorimetric method in our sensing system. A curve of the relationship between ΔI of the SERS and the glucose concentrations (0–100 nM) was obtained as shown in Fig. 5C. The sensing limitation of detection (LOD) of the HSTSN was as low as 0.4 nM (signal-to-noise ratio > 3), evidently lower than the typical LOD of the reported SERS methods [21,22,24,26,42,43], as shown in Table 1.

Interestingly, Fig. 5C shows that the sensing curve was not linear in the whole region, which can be fitted by the three linear calibration lines, namely the line (1) with the largest slope in the concentration range of 0.4–2 nM, the line (2) with the second largest slope in the concentration range of 2–10 nM, and the line (3) with the smallest slope in the range of 10–100 nM. Understandably, the three-segment linear relationships in Fig. 5C were mainly attributed to the great differences in the changes of the *E* among the highly sensitive etching effect of H_2O_2 to the SNTs. According to the simulation results in Fig. 4, small degrees of etching at the tips will induce the sharp drop of the SERS intensity and further etching, the change of SERS intensity will not be very evident. Therefore, the change slop of the SERS intensity in Fig. 5C was gradually decreased due to the gradually decreased influence on the *E* of the SNTs by the etching effects. For further qualitatively analysis, according to the SERS theory [7], SERS intensity can be expressed as:

$$I_{SERS} \propto N \times |E|^4 \quad (3)$$

where I_{SERS} is the intensity of SERS, and *N* is the molecule density on the surface of the SERS tag, *E* is the local electric field mentioned above related to the enhancement of the SERS. When the frequency of incident light is resonant with the LSPR of metal nanoparticles, the redistribution of the *E* results in a giant enhancement of the *E* at a specific position, e.g. the tips of SNTs. Based on the calculations in Fig. 4, when the tips of SNTS are etched, the *E* intensity will be sharply decreased. According to the Eq. (3), the decreased *E* intensity will result in the SERS intensity nonlinear decreased. In addition, according to Eq. (3), I_{SERS} is linearly dependent on *N*. However, the SERS intensity of only the part of *p*-ATP molecules located around the tips is enhanced by the fourth power amplification of the *E*. Therefore, for anisotropic noble mental nanoparticles (such as nanotriangles) with anisotropic *E* distribution, even for label-free SERS sensing, the SERS signal may be not linear with the adding concentration of the analyte, because the analyte may fall into different region on nanoparticles, such as the area far from the tips of SNTs, which will affect the SERS signal differently depending on whether the molecules are close to the tips. Therefore, for anisotropic noble mental nanoparticles, the relationship between I_{SERS} and the concentration of analyte may be not linear, which need to be carefully checked.

3.4. Selectivity of the SERS based HSTSN

To evaluate the selectivity of the HSTSN to glucose recognition, we also compared the responses of the SERS of the HSTSN to other glucose analogues (fructose, maltose, sucrose, starch). Changes in the intensity of the SERS were obtained after separately incubating with these glucose analogues for ca.60 min, as shown in Fig. 6. It can be seen that, in addition to the two groups for glucose and serum glucose, the SERS intensity of HSTSN nearly remained unchanged even if the concentration of other glucose analogues was as high as 500 μM. The high selectivity of HSTSN to glucose recognition can be attributed to the special catalytic ability of GOx to glucose. In addition, in contrast to the label-free SERS detection system, we only need to observe the changes in the intensity of SERS without distinguishing very weak and complex Raman spectral information between glucose and other glucose analogues. This is more convenient for practical applications.

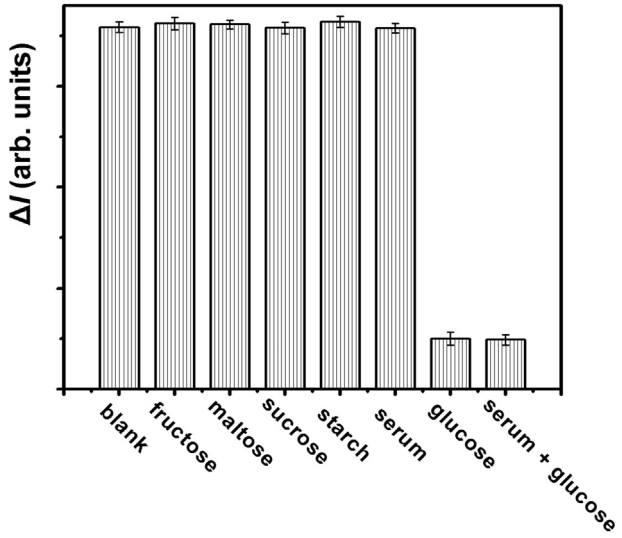

Fig. 6. Change (ΔI) of the SERS intensity of the HSTSN (SNTs concentration ~0.028 nM) incubated with blank (control), fructose (500 μM), maltose (500 μM), sucrose (500 μM), and starch (500 μM), serum (100-fold diluted), glucose (100 μM), and serum (100-fold diluted) contained glucose (100 μM), respectively.

4. Conclusions

In summary, based on capturing glucose by GOx and the resulting enzymatic oxidation reaction to attenuate the local electric field of tips of the SERS tags, the detection system achieved highly sensing of glucose. Associated with the fast decaying of SERS signal due to the dependence of SERS intensity on fourth power *E*, the detection limitation of glucose is as low as 0.4 nM with the sharp decrease of the local electric field intensity as etching the tips. To the best of our knowledge, the observed LOD of glucose is the lowest among the other reported SERS methods. Glucose was successfully detected with good sensitivity and selectivity based on the homogeneous SERS nanoplatform. Moreover, the SERS sensing process only need to monitor the changes of the signal intensity, rather than distinguishing complex Raman spectral information, which is more convenient for practical applications. In addition, our work denoted that, for anisotropic noble mental nanoparticles, the relationship between the concentration and the detection signal may be nonlinearly dependent, which need to be carefully checked. The current work not only demonstrates the great promise of sensing glucose but also provides an interesting approach to design SERS sensing system for other biomolecules with small scattering cross section.

Acknowledgements

This work is financially supported by the National Natural Science Foundation of China (Grant Nos. 61575194, 11874354, 11604331, 11874355, 51772122, 61605130, 61875191 and 11674316). Shenzhen Basic Research Project (JCYJ20180305125425815), China Postdoctoral Science Foundation (2018M643143, 2018M643163). Project of Science and Technology Agency, Jilin Province (20180101222JC).

Declaration of Competing Interest

The author(s) declare that they have no competing interests.

Appendix A. Supplementary data

Supplementary data to this article can be found online at https://doi.org/10.1016/j.apsusc.2019.07.053.

References

[1] K. Furuyama, S. Chera, L. van Gurp, D. Oropeza, L. Ghila, N. Damond, H. Vethe, J.A. Paulo, A.M. Joosten, T. Berney, D. Bosco, C. Dorrell, M. Grompe, H. Raeder, B.O. Roep, F. Thorel, P.L. Herrera, Diabetes relief in mice by glucose-sensing insulin-secreting human alpha-cells, Nature 567 (2019) 43–48, https://doi.org/10.1038/s41586-019-0942-8.

[2] J.L. Harding, M.E. Pavkov, D.J. Magliano, J.E. Shaw, E.W. Gregg, Global trends in diabetes complications: a review of current evidence, Diabetologia 62 (2019) 3–16, https://doi.org/10.1007/s00125-018-4711-2.

[3] M.S. Steiner, A. Duerkop, O.S. Wolfbeis, Optical methods for sensing glucose, Chem. Soc. Rev. 40 (2011) 4805–4839, https://doi.org/10.1039/c1cs15063d.

[4] L.A. Lane, X.M. Qian, S.M. Nie, SERS nanoparticles in medicine: from label-free detection to spectroscopic tagging, Chem. Rev. 115 (2015) 10489–10529, https://doi.org/10.1021/acs.chemrev.5b00265.

[5] C. Zong, M.X. Xu, L.J. Xu, T. Wei, X. Ma, X.S. Zheng, R. Hu, B. Ren, Surface-enhanced Raman spectroscopy for bioanalysis: reliability and challenges, Chem. Rev. 118 (2018) 4946–4980, https://doi.org/10.1021/acs.chemrev.7b00668.

[6] H. Jung, M. Park, M. Kang, K.H. Jeong, Silver nanoislands on cellulose fibers for chromatographic separation and ultrasensitive detection of small molecules, Light Sci. Appl. 5 (2016) e16009, , https://doi.org/10.1038/lsa.2016.9.

[7] Y.Q. Wang, B. Yan, L.X. Chen, SERS tags: novel optical nanoprobes for bioanalysis, Chem. Rev. 113 (2013) 1391–1428, https://doi.org/10.1021/cr300120g.

[8] Y.J. Liu, C.X. Xu, J.F. Lu, Z. Zhu, Q.X. Zhu, A.G. Manohari, Z.L. Shi, Template-free synthesis of porous ZnO/Ag microspheres as recyclable and ultra-sensitive SERS substrates, Appl. Surf. Sci. 427 (2018) 830–836, https://doi.org/10.1016/j.apsusc.2017.07.229.

[9] C. Zhang, C.H. Lia, J. Yu, S.Z. Jiang, S.C. Xu, C. Yang, Y.J. Liu, X.G. Gao, A.H. Liu, B.Y. Man, SERS activated platform with three-dimensional hot spots and tunable nanometer gap, Sensors Actuators B Chem. 258 (2018) 163–171, https://doi.org/10.1016/j.snb.2017.11.080.

[10] C. Zhang, S.Z. Jiang, Y.Y. Huo, A.H. Liu, S.C. Xu, X.Y. Liu, Z.C. Sun, Y.Y. Xu, Z. Li, B.Y. Man, SERS detection of R6G based on a novel graphene oxide/silver nanoparticles/silicon pyramid arrays structure, Opt. Express 23 (2015) 24811–24821, https://doi.org/10.1364/oe.23.024811.

[11] K. Whang, J.H. Lee, Y. Shin, W. Lee, Y. Kim, D. Kim, L.P. Lee, T. Kang, Plasmonic bacteria on a nanoporous mirror via hydrodynamic trapping for rapid identification of waterborne pathogens, Light Sci. Appl. 7 (2018) 68, , https://doi.org/10.1038/s41377-018-0071-4.

[12] N. Bhardwaj, S.K. Bhardwaj, D. Bhatt, D.K. Lim, K.H. Kim, A. Deep, Optical detection of waterborne pathogens using nanomaterials, TrAC Trends Anal. Chem. 113 (2019) 280–300, https://doi.org/10.1016/j.trac.2019.02.019.

[13] B. Ankudze, B. Asare, S. Goffart, A. Koistinen, T. Nuutinen, A. Matikainen, S.S. Andoh, M. Roussey, T.T. Pakkanen, Hydraulically pressed silver nanowire-cotton fibers as an active platform for filtering and surface-enhanced Raman scattering detection of bacteria from fluid, Appl. Surf. Sci. 479 (2019) 663–668, https://doi.org/10.1016/j.apsusc.2019.02.067.

[14] F. Lussier, D. Missirlis, J.P. Spatz, J.F. Masson, Machine-learning-driven surface-enhanced Raman scattering optophysiology reveals multiplexed metabolite gradients near cells, ACS Nano 13 (2019) 1403–1411, https://doi.org/10.1021/acsnano.8b07024.

[15] L. Rodriguez-Lorenzo, L. Fabris, R.A. Alvarez-Puebla, Multiplex optical sensing with surface-enhanced Raman scattering: a critical review, Anal. Chim. Acta 745 (2012) 10–23, https://doi.org/10.1016/j.aca.2012.08.003.

[16] H.N. Lin, C.S. Liao, P. Wang, N. Kong, J.X. Cheng, Spectroscopic stimulated Raman scattering imaging of highly dynamic specimens through matrix completion, Light Sci. Appl. 7 (2018) 17179, , https://doi.org/10.1038/lsa.2017.179.

[17] W. Yang, Z. Li, Z.Y. Lu, J. Yu, Y.Y. Huo, B.Y. Man, J. Pan, H.P. Si, S.Z. Jiang, C. Zhang, Graphene-Ag nanoparticles-cicada wings hybrid system for obvious SERS performance and DNA molecular detection, Opt. Express 27 (2019) 3000–3013, https://doi.org/10.1364/oe.27.003000.

[18] J.H. Xu, C.H. Li, H.P. Si, X.F. Zhao, L. Wang, S.Z. Jiang, D.M. Wei, J. Yu, X.W. Xiu, C. Zhang, 3D SERS substrate based on Au-Ag bi-metal nanoparticles/MoS2 hybrid with pyramid structure, Opt. Express 26 (2018) 21546–21557, https://doi.org/10.1364/oe.26.021546.

[19] Y. Guo, J. Yu, C.H. Li, Z. Li, J. Pan, A.H. Liu, B.Y. Man, T.F. Wu, X.W. Xiu, C. Zhang, SERS substrate based on the flexible hybrid of polydimethylsiloxane and silver colloid decorated with silver nanoparticles, Opt. Express 26 (2018) 21784–21796, https://doi.org/10.1364/oe.26.021784.

[20] D.A. Stuart, J.M. Yuen, N.S.O. Lyandres, C.R. Yonzon, M.R. Glucksberg, J.T. Walsh, R.P. Van Duyne, In vivo glucose measurement by surface-enhanced Raman spectroscopy, Anal. Chem. 78 (2006) 7211–7215, https://doi.org/10.1021/ac061238u.

[21] K.P. Sooraj, M. Ranjan, R. Rao, S. Mukherjee, SERS based detection of glucose with lower concentration than blood glucose level using plasmonic nanoparticle arrays, Appl. Surf. Sci. 447 (2018) 576–581, https://doi.org/10.1016/j.apsusc.2018.04.020.

[22] K.V. Kong, C.J.H. Ho, T.X. Gong, W.K.O. Lau, M. Olivo, Sensitive SERS glucose sensing in biological media using alkyne functionalized boronic acid on planar substrates, Biosens. Bioelectron. 56 (2014) 186–191, https://doi.org/10.1016/j.bios.2013.12.062.

[23] B. Sharma, P. Bugga, L.R. Madison, A.I. Henry, M.G. Blaber, N.G. Greeneltch, N.H. Chiang, M. Mrksich, G.C. Schatz, R.P. Van Duyne, Bisboronic acids for selective, physiologically relevant direct glucose sensing with surface-enhanced Raman spectroscopy, J. Am. Chem. Soc. 138 (2016) 13952–13959, https://doi.org/10.1021/jacs.6b07331.

[24] Q.L. Chen, Y. Fu, W.H. Zhang, S.B. Ye, H. Zhang, F.Y. Xie, L. Gong, Z.X. Wei, H.Y. Jin, J. Chen, Highly sensitive detection of glucose: a quantitative approach employing nanorods assembled plasmonic substrate, Talanta 165 (2017) 516–521, https://doi.org/10.1016/j.talanta.2016.12.076.
[25] D. Yang, S. Afroosheh, J.O. Lee, H. Cho, S. Kumar, R.H. Siddique, V. Narasimhan, Y.Z. Yoon, A.T. Zayak, H. Choo, Glucose sensing using surface-enhanced Raman-mode constraining, Anal. Chem. 90 (2018) 14269–14278, https://doi.org/10.1021/acs.analchem.8b03420.
[26] L. Perez-Mayen, J. Oliva, P. Salas, E. De la Rosa, Nanomolar detection of glucose using SERS substrates fabricated with albumin coated gold nanoparticles, Nanoscale 8 (2016) 11862–11869, https://doi.org/10.1039/c6nr00163g.
[27] Q.H. Zeng, Y.L. Zhang, X.M. Liu, L.P. Tu, X.G. Kong, H. Zhang, Multiple homogeneous immunoassays based on a quantum dots-gold nanorods FRET nanoplatform, Chem. Commun. 48 (2012) 1781–1783, https://doi.org/10.1039/c2cc16271g.
[28] S.S. Acimovic, H. Sipova, G. Emilsson, A.B. Dahlin, T.J. Antosiewicz, M. Kall, Superior LSPR substrates based on electromagnetic decoupling for on-a-chip high-throughput label-free biosensing, Light Sci. Appl. 6 (2017) e17042, , https://doi.org/10.1038/lsa.2017.42.
[29] W. Kusnezow, Y.V. Syagailo, S. Ruffer, K. Klenin, W. Sebald, J.D. Hoheisel, C. Gauer, I. Goychuk, Kinetics of antigen binding to antibody microspots: strong limitation by mass transport to the surface, Proteomics 6 (2006) 794–803, https://doi.org/10.1002/pmic.200500149.
[30] D.M. Jameson, J.A. Ross, Fluorescence polarization/anisotropy in diagnostics and imaging, Chem. Rev. 110 (2010) 2685–2708, https://doi.org/10.1021/cr900267p.
[31] J.J. Wang, X.Y. Huang, H. Liu, C.Q. Dong, J.C. Ren, Fluorescence and scattering light cross correlation spectroscopy and its applications in homogeneous immunoassay, Anal. Chem. 89 (2017) 5230–5237, https://doi.org/10.1021/acs.analchem.6b04547.
[32] X.L. Wang, S. Niazi, H. Yukun, W.J. Sun, S.J. Wu, N. Duan, X. Hun, Z.P. Wang, Homogeneous time-resolved FRET assay for the detection of Salmonella typhimurium using aptamer-modified $NaYF_4$: Ce/Tb nanoparticles and a fluorescent DNA label, Microchim. Acta 184 (2017) 4021–4027, https://doi.org/10.1007/s00604-017-2399-5.
[33] Q. Yu, P.L. Gao, K.Y. Zhang, X. Tong, H.R. Yang, S.J. Liu, J. Du, Q. Zhao, W. Huang, Luminescent gold nanocluster-based sensing platform for accurate H2S detection in vitro and in vivo with improved anti-interference, Light Sci. Appl. 6 (2017) e17107, , https://doi.org/10.1038/lsa.2017.107.
[34] Y. Wang, L.J. Tang, J.H. Jiang, Surface-enhanced Raman spectroscopy-based, homogeneous, multiplexed immunoassay with antibody-fragments-decorated gold nanoparticles, Anal. Chem. 85 (2013) 9213–9220, https://doi.org/10.1021/ac4019439.
[35] Q. Zhang, N. Li, J. Goebl, Z. Lu, Y. Yin, A systematic study of the synthesis of silver nanoplates: is citrate a “magic” reagent? J. Am. Chem. Soc. 133 (2011) 18931–18939.
[36] Y.F. Huang, D.Y. Wu, H.P. Zhu, L.B. Zhao, G.K. Liu, B. Ren, Z.Q. Tian, Surface-enhanced Raman spectroscopic study of p-aminothiophenol, Phys. Chem. Chem. Phys. 14 (2012) 8485–8497, https://doi.org/10.1039/c2cp40558j.
[37] M. Osawa, N. Matsuda, K. Yoshii, I. Uchida, Charge transfer resonance Raman process in surface-enhanced Raman scattering from p-aminothiophenol adsorbed on silver: Herzberg—Teller contribution, J. Phys. Chem. 98 (1994) 12702–12707, https://doi.org/10.1021/j100099a038.
[38] R. Jin, Y. Cao, C.A. Mirkin, K. Kelly, G.C. Schatz, J. Zheng, Photoinduced conversion of silver nanospheres to nanoprisms, Science 294 (2001) 1901–1903.
[39] B. Xue, D. Wang, J. Zuo, X.G. Kong, Y.L. Zhang, X.M. Liu, L.P. Tu, Y.L. Chang, C.X. Li, F. Wu, Q.H. Zeng, H.F. Zhao, H.Y. Zhao, H. Zhang, Towards high quality triangular silver nanoprisms: improved synthesis, six-tip based hot spots and ultra-high local surface plasmon resonance sensitivity, Nanoscale 7 (2015) 8048–8057, https://doi.org/10.1039/c4nr06901c.
[40] H.L. He, X.L. Xu, H.X. Wu, Y.J. Zhai, Y.D. Jin, In situ nanoplasmonic probing of enzymatic activity of monolayer-confined glucose oxidase on colloidal nanoparticles, Anal. Chem. 85 (2013) 4546–4553, https://doi.org/10.1021/ac4001805.
[41] Q. Zhang, C.M. Cobley, J. Zeng, L.P. Wen, J.Y. Chen, Y.N. Xia, Dissolving Ag from Au-Ag alloy nanoboxes with H_2O_2: a method for both tailoring the optical properties and measuring the H_2O_2 concentration, J. Phys. Chem. C 114 (2010) 6396–6400, https://doi.org/10.1021/jp100354z.
[42] G.H. Qi, Y. Wang, B.Y. Zhang, D. Sun, C.C. Fu, W.Q. Xu, S.P. Xu, Glucose oxidase probe as a surface-enhanced Raman scattering sensor for glucose, Anal. Bioanal. Chem. 408 (2016) 7513–7520, https://doi.org/10.1007/s00216-016-9849-5.
[43] J.A. Kwon, C.M. Jin, Y. Shin, H.Y. Kim, Y. Kim, T. Kang, I. Choi, Tunable plasmonic cavity for label-free detection of small molecules, ACS Appl. Mater. Interfaces 10 (2018) 13226–13235, https://doi.org/10.1021/acsami.8b01550.